AN APPROACH FOR ACCURATE MEASUREMENT OF FRACTAL DIMENSION DISTRIBUTION ON FRACTURE SURFACES

Petr FRANTÍK[1]

[1]Institute of Structural Mechanics, Faculty of Civil Engineering, Brno University of Technology, Veveří 331/95, Brno, Czech Republic

kitnarf@centrum.cz

DOI: 10.35181/tces-2022-0002

Abstract. *The paper describes a new approach to measuring the box-counting fractal dimension of surfaces based on making cuts and using the walking divider method with an improvement. The method is applied on a surface created by the fracture of an artificial composite. It is usable for accurate estimation of fractal dimension of flatter surfaces for which it is necessary to measure with small deviation. It also allows the discovery of the dimension distribution along the surface.*

Keywords

Fractal dimension, fracture, distribution, cement composite.

1. Introduction

A fractal dimension of an object is a ratio describing how some geometric measure depends on a scale by which the object is measured. Fractal dimension, also described by its inventor as similarity exponent [1], plays an essential role for generic objects – fractals – exhibiting so-called self-similarity. Self-similarity of an object means that a pattern on the (ideal) object is present on all geometrical scales. Especially fractal functions have fascinating and long mathematical history directly connected with great and innovative mathematicians, namely Bernard Bolzano (~1831, Bolzano's continuous and non-differentiable function), Georg Cantor (1874, Cantor set) and Karl Weierstrass (1872, Weierstrass function). The term fractal, systematic study, and establishment of fractal geometry, including its application to ideal and natural objects, originates in the work of Benoit Mandelbrot [1, 2]. Note that Mandelbrot cited the discovery of Lewis Richardson during measuring of length of a coastline, see [1], where the fractal (originally fractional) dimension and method of its measuring were defined. Term fractal dimension currently represents many fractal dimensions with different definitions and uses in many scientific disciplines [3, 4, 5, 6, 7]. Also, methods for measuring those dimensions and their accuracy differ significantly.

Real-world fractals show statistical self-similarity. Objects can be typically so-called multifractals due to an inherent dependency of some object property on a scale which causes dependency of fractal dimension on the scale. See [8] for references about methods for accurate handling of multifractals.

It becomes apparent that it is easy to find an object or process which has or produces some form of such apparent irregularity on particular scales. Ideal simple geometric objects with differentiable surfaces are not as common as we expected or believe. Let us mention that our (human) perception system tends to simplify the shape of all objects available for perception. Our brain represents/models observed objects in some ideal form, e.g. [9].

The surfaces of natural and artificial materials created by fracture are considered fractal objects. A typical and massively used artificial material in civil engineering is a cement composite, commonly verified in fracture tests to determine fracture properties. These properties are then used to create material models for numerical calculations of the expected response of an engineering structure made of such material. The measurement of the fractal dimension of the fracture surfaces created in these tests can be considered independent and can help to understand the fracture process. Many authors deal with the characterization of fracture surfaces of cement composites from the point of view of fractal dimension determination and its correlation to other materials parameters, e.g. [10, 11, 12, 13, 14, 15].

Unfortunately, the fracture surface of cement concrete is typically flatter, which means that the surface can be reliably defined as a two-dimensional function, and the measured fractal dimension is often very close to the topological dimension, see [13, 15]. This fact makes the task highly sensitive and requires very accurate

measurement. The developed method described in this paper is used for measuring the box-counting dimension d, generally defined [7]:

$$d = \frac{\ln\left(\frac{N_b}{N_a}\right)}{\ln\left(\frac{L_a}{L_b}\right)}, \quad (1)$$

where N_i is a count of generalized boxes of size L_i covering a measured object. The symbols a and b represent bounds of scales where the object is defined. We expect the object to be a fractal with a single box-counting dimension within these bounds.

Measuring the fractal dimension of a one-dimensional function made by a cut of a fracture surface is used because of the possibility of enhancing accuracy and discovering changes in fractal properties along with fracture evolution. The original Walking divider method [16, 17] designed to measure the box-counting dimension is significantly improved in this paper for accuracy and applied on a fracture surface. According to the definition above, both the classical and improved methods cover a one-dimensional function $h(x)$ by a number N of line segments of length L.

2. Method

As was mentioned, assume that we have a relatively flatter surface represented as a function $z = f(x,y)$ on a rectangular area, see Fig. 1. We will measure fractal dimensions d_x, d_y of cuts of the function f made by planes perpendicular to axes x and y. For example, dimension $d_x(y_c)$ of one-dimensional function $z = f_x(x) \mid y = y_c$ obtained by cutting a plane perpendicular to axis y which intersects this axis at point $y = y_c$. The improved walking divider method, described in detail below, will measure the fractal dimensions $d_x(y_c)$ and $d_y(x_c)$. After calculation of those dimensions we will calculate cross-dimension value $d_c(x_c, y_c) = \left(d_x(y_c) + d_y(x_c)\right)/2$.

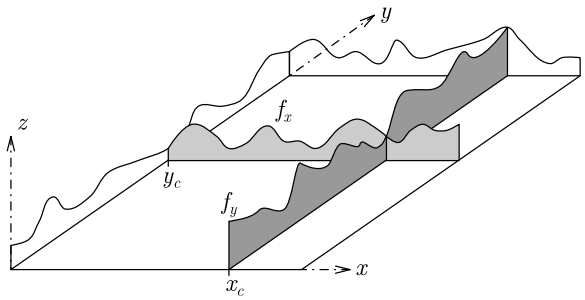

Fig. 1: A surface defined on a rectangular area and its perpendicular cuts.

2.1. Improved Walking divider

For the sake of simplicity assume a continuous one-dimensional function $z = h(x)$ defined on interval (a,b). The new method will fully cover the function h by a sorted set $P(h)$ of line polygonal functions p_i, each with a particular count of segments N_i of length L_i, $L_i > L_{i+1}$, where $i = 1, 2, \ldots, n$ is an index of the polygon, see Fig. 2.

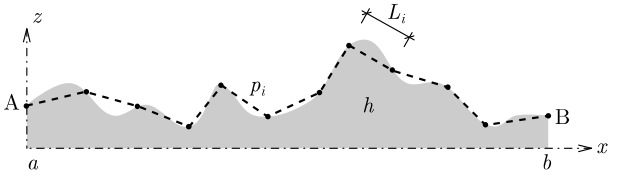

Fig. 2: Function h is covered by polygonal function p_i with segments of length L_i on the interval (a,b).

The algorithm searches for polygons with line segments of the spatial length L_i and with vertices lying on the function $h(x)$. Length L_i is a constant for a particular polygon p_i. Note that the polygon must cover the whole interval, which is the key improvement of the original method [16]. I.e. each polygon begins in point A=$(a,h(a))$ and ends in B=$(b,h(b))$.

The first polygon p_0, not included in the set $P(h)$, with the largest segment length $L_0 = L_{\max}$, has only a single line segment connecting points A and B, see Fig. 3. It is based on the assumption that the function h is flat enough so that a polygon with more segments with the same or a larger segment length L does not exist. The segment has the length L_0, which is equal to the distance between the first and the last point of the measured function h:

$$L_0 = \sqrt{(h(b) - h(a))^2 + (b-a)^2} \approx b - a. \quad (2)$$

The second polygon p_1, with segment length L_1, can also be easily found. The length L_1 is the distance between an intersection of a crossing line and the point A or B. The crossing line is perpendicular to the polygon p_0 and going through its midpoint, see Fig. 3. In general, there can be more than a single polygon p_1, but the solution will be unique, considering a flatter surface.

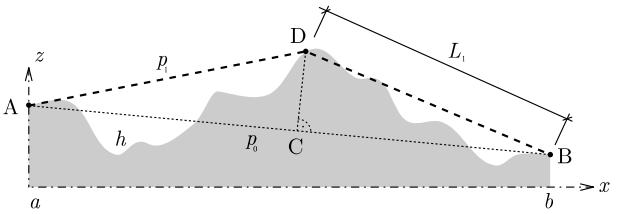

Fig. 3: The first and the second polygon cover the function h.

The middle vertex of the polygon p_1 can be found in two ways. The first procedure creates intersection point D using a line through the center of p_0 (marked in Fig. 3 as C) perpendicular to the polygon p_0. The second procedure rotates function h, so the line segment p_0 will be horizontal and search for value z^* of rotated function h^* at the transformed midpoint coordinate x^*. The intersection point (x^*, z^*) is then transformed back. Note that the intersection point will be close to coordinate $x = 0.5(b-a)$. In this case, the length L_1 can be approximated by:

$$L_1 \approx \sqrt{\left(h\left(a + \frac{b-a}{2}\right) - h(a)\right)^2 + \left(\frac{b-a}{2}\right)^2}. \quad (3)$$

Researchers [16, 17] recommended not to use polygon p_0 due to its influence on the estimated dimension, and this influence was numerically verified. The improved method does not include polygon p_0 in the set $P(h)$. Emphasize that the original method [16, 17] is designed to search for polygons in the opposite direction.

In contrast to L_{max}, the smallest length L_{min} can be unknown and must be determined if the function h is known only at discrete points and intermediate values are interpolated. The following relationship can approximate the lower boundary of L_{min}:

$$L_{min} \geq s_{max}, L_{min} \approx \sqrt{2}\max_k(x_{k+1} - x_k), \quad (4)$$

where s_{max} is the largest spatial distance between neighboring points and k is the index in the sorted sequence of discrete points in which the function h is known. The constant $\sqrt{2}$ in the relationship (4) is based on the assumption that the function h is flat enough, which means that neighboring points of the discretized function h will not have a slope higher than 1. It is more reliable to use a higher value for this constant because of the calculation deviation caused by the measurement being too close to the discretization step. Note that work [16] uses a constant 0.5, which is typically too small and causes a bias in the dimension estimate.

The fractal dimension is measured as the slope of the linear approximation $\tilde{u}$ of the log-log plot of the dependency between the polygon segment count and the segment length. Define substitution for a clearer description:

$$u_i = \ln\left(\frac{L_1}{L_i}\right),\ v_i = \ln(N_i), \quad (5)$$

in which $\{u_i, v_i \mid i = 1, 2, \ldots, n\}$ represent set of values of properties of all polygons from the set $P(h)$ transformed for the plot. The approximation $\tilde{u}(v)$ is usually made by least squares method based on calculation of sum of squares of deviations:

$$J(d, q, \{u_i, v_i\}) = \sum_{i=1}^{n}(du_i + q - v_i)^2, \quad (6)$$

where J is a least-square deviation function dependent on two approximation parameters d, q, and a set of values of polygon properties $\{u_i,v_i\}$. The value d is a slope of the linear approximation $\tilde{u}$, the estimated fractal dimension, and q is a shift. The deviation is then minimized, which gives known relationships:

$$d = \frac{n\sum(u_i v_i) - \sum u_i \sum v_i}{\sum u_i^2 - (\sum u_i)^2},$$
$$q = \frac{\sum u_i^2 \sum v_i - \sum u_i \sum u_i v_i}{\sum u_i^2 - (\sum u_i)^2}. \quad (7)$$

Unfortunately, the set $P(h)$ of all existing polygons has asymmetric distribution, similar to geometric sequence, due to more frequent polygons near the lower boundary L_{min} and rare polygons near L_{max}. The dimension estimate d is biased due to this irregular distribution.

Let us define a new approximation $\tilde{u}_s(v)$ of a new set $P_s(h)$ made by sampling from the set $P(h)$ to ensure approximate regularity of the polygon distribution in all scales in the log-log plot $\{u_i,v_i\}$. A new set $\{u_j, v_j\}$ made by sampling from $\{u_i, v_i\}$ can be created by searching polygons with a sampling interval of logarithmic length g, estimated as the difference between segment lengths L_1 and L_2:

$$g = \ln\left(\frac{1}{L_2}\right) - \ln\left(\frac{1}{L_1}\right) = \ln\left(\frac{L_2}{L_1}\right), \quad (8)$$

where L_2 is the segment length of the third existing polygon p_2, which must be found numerically, e.g., by the modified bisection method.

As the first step of the numeric method, there is a logical assumption that polygon p_2 can exist with $N_2 = 3$. With this assumption, the following must apply:

$$L_1 \geq \frac{L_0}{2},\ L_2 \geq \frac{2}{3}L_1,\ L_2 \geq \frac{L_0}{3}. \quad (9)$$

Note that polygon p_2 with $N_2 = 3$ may not exist. If it does not exist, then continue the search for $N_2 = 4$ and so on, with a generalized formula for polygon p_2:

$$\frac{L_2}{L_0} \geq \frac{1}{N_2},\ L_2 \geq \frac{L_0}{N_2}. \quad (10)$$

With knowledge of the polygon p_2 and the value of logarithmic distance g we can have three fundamentally different approaches how to get the set $P_s(h)$:

a) find the set of all existing polygons $P(h)$ and make $P_s(h)$ using a sampling (brute force method),

b) find polygons around $L_{sj} = L_1 e^{-(j-1)g}, j = 3,4,\ldots,n_s$

c) ditto around $N_{sj} = N_1 e^{(j-1)g}$,

where n_s is the number of polygons in the set $P_s(h)$. Note that searching for polygons close to equidistantly distributed coordinates v is similar to the original procedure [16], using an exact geometric sequence to determine segment lengths L. However, polygons with those lengths do not cover the function exactly, which leads to biased estimation.

When the set $P_s(h)$ has been found and parameters d_s, q_s of linear approximation $\tilde{u}_s(v)$ determined using relationship (7) adapted for P_s, the standard deviation of the dimension d_s can be calculated using the known relationship:

$$\sigma_{ds} = \sqrt{\frac{1}{n_s - 2}\frac{\sum(v_j - du_j - q_s)^2}{\sum\left(u_j - \frac{1}{n}\sum u_j\right)^2}}. \quad (11)$$

Finally, we can write the fractal dimension in the form:

$$d_s \pm \sigma_{ds} \quad (12)$$

2.2. Area scan

As described above, using the described method, we can calculate the cross-dimension function $d_c(x_c,y_c)$ for any continuous function $f(x,y)$. The function $d_c(x_c,y_c)$ can be used to locate some fractal dimension disturbances, and the result can be further enriched and verified. It is possible to divide the area into subareas and measure cross-dimension $d_c(x_c,y_c)$. We can expect better localization of disturbances in smaller areas, see Fig. 4, along with

some verification from results taken on larger areas. Note that when we have only discrete points of function *f*, the smaller areas, taken from the original discretization, will probably have higher standard deviations because of lower counts of known points. We suggest dividing the area into regular subareas of shapes close to a square to keep the unbiased dimension measurement in both directions.

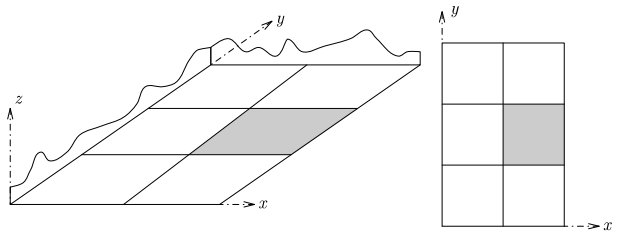

Fig. 4: Measurement of cross-dimension on subareas.

3. Application

The method described above was applied on a fracture surface originating by fracture caused by bending a notched concrete specimen, marked as W_100_L_1_A, loaded in the three-point bending test. For more details, see publication [18]. After the fracture test, the whole surface of one side of the ligament of the specimen of size approximately 98×49 mm was measured by a laser profilometer with sampling step 50 μm in both directions, which gives a grid of size 1960×989 points. The surface is plotted in Fig. 5 using color-coding.

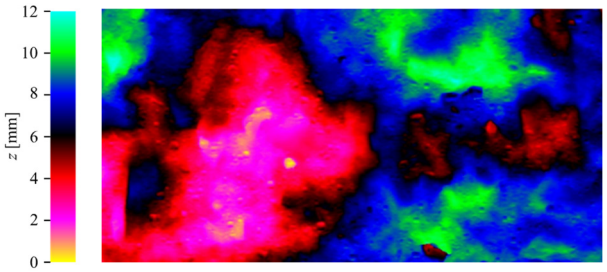

Fig. 5: The fracture surface of the ligament of specimen W_100_L_1_A

In Fig. 5 we can see that the coordinate *z* of the scanned surface varies between 0 and 12 mm. Coordinates *z* are coded using colors. The values at the bottom part are continuously coded from black to red, magenta, and yellow (the black color is on mid-level). At the top part, from black to blue, green, and cyan.

3.1. Fractal dimension

For the presentation of improved walking divider method performance, the first top row from the grid was taken, see Fig. 6, and is available on the web [19]. In this row, the fractal dimension calculation using the described method was made, resulting in the value 1.0251 ± 0.0013. The corresponding graph of the polygons found shown in Fig. 7.

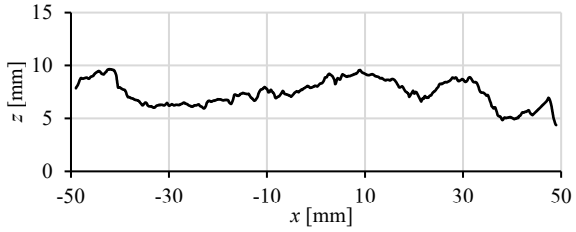

Fig. 6: The top row of the scanned grid (data are available at [19]).

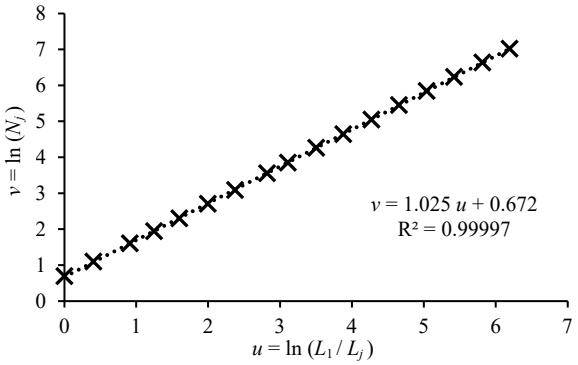

Fig. 7: Graph of the plotted polygons found (crosses) and their linear approximation (dotted line).

Tab. 1: The table of the plotted polygons (displayed in Fig. 7) with the list of values of calculated search points L_{sj}, N_{sj} for the selected function.

j	L_j	N_j	L_{sj}	N_{sj}
1	49.044	2	ditto	ditto
2	32.739	3	ditto	ditto
3	19.721	5	21.855	4
4	14.080	7	14.589	7
5	9.913	10	9.739	10
6	6.672	15	6.501	15
7	4.560	22	4.340	23
8	2.928	35	2.897	34
9	2.188	47	1.934	51
10	1.476	71	1.291	76
11	1.014	104	0.862	114
12	0.686	156	0.575	171
13	0.467	233	0.384	255
14	0.318	346	0.256	383
15	0.217	512	0.171	573
16	0.147	762	0.114	859
17	0.100	1117	0.076	1286

In Fig. 7 can be seen the accuracy of the result of measurement of all quantities such that there is no visible deviation from line approximation. Note that there are not enough polygons to keep exact equidistant distribution at some intervals. Described brute force variant was used to find all 547 exact polygons (until the bottom limit L_{min} was reached) from which the set of points $\{L_i,N_i\}$ was selected. Furthermore, Tab. 1 also presents search values L_{si} and N_{si} calculated using the relationships described above. The list of all polygons is also available at [19].

3.2. Cross-dimension and subareas

Remind that calculating a fractal dimension distribution needs processing of every row and column of the grid. Two applications will be presented here on the scanned surface as a whole and the surface divided into 16×8 subareas for better spatial accuracy.

Whole surface scanning gave a minimal fractal dimension 1.0155 ± 0.0009, a maximal 1.051 ± 0.004, and the largest standard deviation 0.0041 measured on rows. On columns was found a minimal value 1.0243 ± 0.0017, a maximal 1.092 ± 0.006, and the largest standard deviation 0.013. Cross-dimension varies between 1.02 and 1.07 with modus 1.0317, see Fig. 8 and Fig. 9.

On 16×8 subareas, cross-dimension varies between 1.005 and 1.35 with modus 1.0326 (Fig. 8 and Fig. 10). The highest values form islands which are suspected of some deviations on the fracture surface. In Fig. 11 can be seen that those islands probably correspond with high values of magnitudes of gradients of the discretized fracture surface or with derivatives of those gradients. Those islands indicate the existence of localized different structures on the fracture surface.

Note that distributions of dimensions in Fig. 8 reflect the fact that localization of measurement will affect the variance of dimension values because of the nature of the calculation method. More precisely, the measurement has an averaging effect such that larger areas will probably have smaller variance, as seen in Fig. 8.

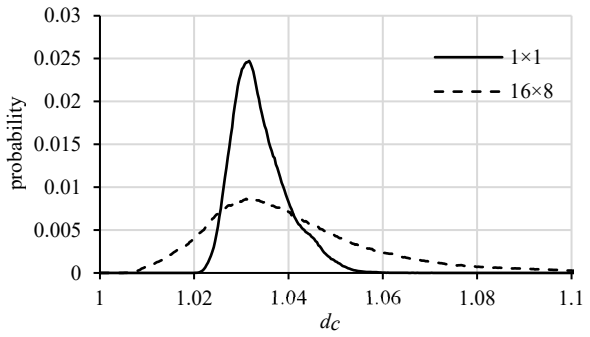

Fig. 8: The probability distribution function of cross-dimension d_c for both area measurements).

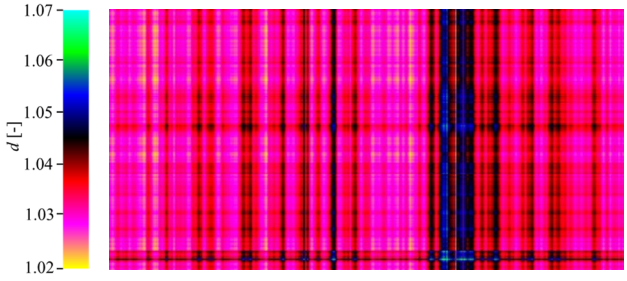

Fig. 9: Distribution of cross-dimension d_c measured on the whole surface.

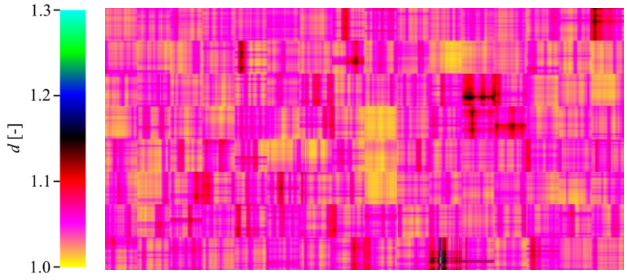

Fig. 10: Distribution of cross-dimension d_c measured on 16×8 subareas.

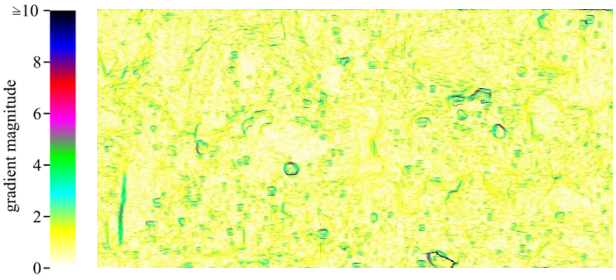

Fig. 11: The color-coded magnitudes of discretized surface gradients. Those numbers are defined only for the particular discretization of the surface.

4. Conclusion

This paper introduces a new approach to accurately measuring the fractal dimension of fracture surfaces, which are typically relatively flatter with an estimated fractal dimension close to the topological dimension. The approach was based on using one-dimensional functions produced by cuts of measured surfaces which can be used along with an improved walking divider method. For the particular surface obtained from the fracture test, it was shown that the fractal dimension of cuts did not overstep the value of approximately 1.1 except on areas recognizable as deviations and described as different structures on the fracture surface. It was presented that those deviations can be predicted by measuring gradients of the discretized fracture surface. Also, dimension distribution along the surface was observed thank this approach.

The notable result is that the modus of cross-dimension distribution is very similar for both area measurements, particularly value 1.0317 for measurement on the whole surface and 1.0326 for 16×8 subareas. Such similarity of modus was not expected, and its possible use will be verified for large sets of samples in the future.

The scanning procedure for obtaining the fracture surface has some adverse effects on the fractal dimension measurement, which will need further investigation. The first known effect is that the surface is scanned in one direction. This problem can be eliminated by scanning in both directions and making a merge. The second effect is that the scanning method is constrained to measure only flatter surfaces, as was defined in the paper, and this

constraint is also direction-dependent.

Acknowledgments

Author wish to thank to Zbyněk Keršner, David Lehký, Jiří Macur, Jakub Sobek, Tomáš Trčka, and Martina Šomodíková with supporting within this work. The research was carried out with the support of the Czech Science Foundation under project 19-09491S (MUFRAS).

References

[1] MANDELBROT, B. How Long Is the Coast of Britain? Statistical Self-Similarity and Fractional Dimension, *Science*, 156 (3775): 636–638, 1967.

[2] MANDELBROT, B. Fractals: Form, Chance and Dimension, by Benoît Mandelbrot; W. H. Freeman and Co, 1977; ISBN 0-7167-0473-0S.

[3] TURNER, J. M., BLACKLEDGE, J. M. and ANDREWS, P. R. Fractal Geometry in Digital Imaging, Academic Press; 1st edition, 1998, 328 pages, ISBN-10: 0127039708.

[4] BERKE, J. Spectral Fractal Dimension, New Mathematics and Natural Computation, 2007.

[5] BUDRONI, M. A., BARONCHELLI, A. & PASTOR-SATORRAS, R. Scale free networks emerging from multifractal time series. Phys. Rev. E 95, 052311, 2017.

[6] XING, Y., SUN, Q., ZHU, M., BAI, J. & WANG, Q. Correlation between anisotropic fractal dimension of fracture surface and coercivity for Nd-Fe-B permanent magnets, J. of Mat. Res. And Tech., 2021.

[7] CATALAN, G., BÉA, H., FUSIL, S., BIBES, M., PARUCH, P., BARTHÉLÉMY, A. & SCOTT, J. F., Fractal dimension and size scaling of domains in thin films of multiferroic BiFeO3, Phys. Rev. Let., 2008.

[8] CREUTZBURG, R. & IVANOV, E. Improving Accuracy in Fractal Dimension Calculation by Multiresolution Approach, Conference Paper in Proceedings of SPIE - The International Society for Optical Engineering, 2000.

[9] BERTHOZ, A. The Human Brain “Projects” upon the World, Simplifying Principles and Rules for Perception. In: Berthoz A., Christen Y. (eds) Neurobiology of “Umwelt”. Research and Perspectives in Neurosciences. Springer, Berlin, Heidelberg, 2009.

[10] SAOUMA, V. E., BARTON, C. C., GAMALELDIN, N. A. Fractal characterization of fracture surfaces in concrete. Engineering Fracture Mechanics, 35, No. 1/2/3, 47 – 53, 1990.

[11] BRANDT, A. M., PROKOPSKI, G. On the fractal dimension of fracture surfaces of concrete elements. Journal of Material Science, 28, 4762 – 4766, 1993.

[12] BAŽANT, Z. P.: Scaling of Quasi-Brittle Fracture and the Fractal Question, Journal of Engineering Materials and Technology, 117, 361-367, 1995.

[13] CARPINTERI, A., CHIAIA, B., INVERNIZZI, S. Three-dimensional fractal analysis of concrete fracture at the meso-level. Theoretical and Applied Fracture Mechanics, 31, 163 – 172, 1999.

[14] CARPINTERI, A., INVERNIZZI, S.: Uniaxial tensile test and fractal evaluation of softening damage in concrete. Fracture Mechanics of Concrete Structures, de Borst et al. (eds), Swets & Zeitlinger, Lisse, ISBN 90 2651 825 0, 19 – 25, 2001.

[15] MECHTCHERINE, V., MULLER, H. S. Fractological investigation on the fracture in concrete. Fracture Mechanics of Concrete Structures, de Borst et al. (eds), Swets & Zeitlinger, Lisse, 2001, ISBN 90 2651 825 0, 81 - 88.

[16] SHELBERG, M.C., MOELLERING, H., and LAM, N. S. Measuring the Fractal Dimensions of Empirical Cartographic Curves. Proceedings, Auto-Carto 5, pp. 481-490, 1982.

[17] TURNER, J. M., BLACKLEDGE, J. M., ANDREWS, P. R. Fractal Geometry in Digital Imaging, Academic Press; 1st edition, 1998, 328 pages, ISBN-10: 0127039708

[18] SOBEK, J., FRANTÍK, P., TRČKA, T., LEHKÝ, D. Fractal Dimension Analysis of Three-Point Bending Concrete Test Specimens, MATEC Web of Conferences 323(107):01011, 2020.

[19] FRANTÍK, P. Online archive. Available on web at http://www.kitnarf.cz/achive/2021/fractdim.zip

About Authors

Petr Frantík was born in Olomouc, Czech Republic. He received his Ph.D. from Brno University of Technology in 2004. His research interests include fractal geometry, nonlinear dynamics, deterministic chaotic and physical discretization.